Journal of MATERIALS RESEARCH

Article
DOI: 10.1557/jmr.2019.81

Impact of linker positions for thieno[3,2-*b*]thiophene in wide band gap benzo[1,2-*b*:4,5-*b*9]dithiophene-based photovoltaic polymers

Mingjing Zhang[1], Xiaofang Zhang[1], Pengzhi Guo[2], Jie Lv[1], Xunchang Wang[3], Junfeng Tong[1,a)], Yangjun Xia[1,b)]

[1]*Key Laboratory of Optoelectronic Technology and Intelligent Control of Ministry Education, Lanzhou Jiaotong University, Lanzhou 730070, People's Republic of China; and School of Materials Science and Engineering, Lanzhou Jiaotong University, Lanzhou 730070, People's Republic of China*
[2]*National Green Coating Technology and Equipment Research Center, Lanzhou Jiaotong University, Lanzhou 730070, People's Republic of China*
[3]*CAS Key Laboratory of Bio-based Materials, Qingdao Institute of Bioenergy and Bioprocess Technology, Chinese Academy of Sciences, Qingdao 266101, China*
[a)]Address all correspondence to these authors. e-mail: tongjf@mail.lzjtu.cn
[b)]e-mail: xiayangjun2015@126.com

Received: 7 November 2018; accepted: 13 February 2019

Two wide band gap conjugated polymers, namely PBDT-TT25 and PBDT-TT36, derived from (4,8-bis(4,5-dioctyl-thiophen-2-yl)benzo[1,2-*b*:4,5-*b*9]dithiophene-2,6-diyl)bis(trimethylstannane) with 2,5-dibromothieno[3,2-*b*]thiophene (TT25) or 3,6-dibromothieno[3,2-*b*]thiophene (TT36), have been synthesized by simply altering the linker positions of thieno[3,2-*b*]thiophene unit. The impact of linker positions on the energy levels, aggregation, active layer morphology, and optical and photovoltaic properties was evaluated systemically. We found that the absorption was greatly broadened, and the highest occupied molecular orbital (HOMO) energy level was elevated as the result of the significantly reduced twist angle on the polymer backbone when the linker positions changed from 3,6-isomer to 2,5-isomer. Therefore, the optimal inverted polymer solar cells exhibited a 1.87 times enhancement in power conversion efficiencies (PCE), which was mainly ascribed to the higher short circuit current densities (J_{SC}) and fill factor (FF) of the devices mainly benefited from the widened, stronger absorption, higher hole mobility, and more ordered structure.

Introduction

Polymer solar cells (PSCs) with bulk heterojunction structures have attracted significant attention due to their advantages of light weight, low cost, and elasticity in large area applications by inkjet printing and roll-to-roll solution processes [1, 2, 3, 4]. Typically, the key component of PSCs, photoactive blend layer, consists of p-type conjugated polymers (CPs) as electron donor and n-type electron acceptor materials, sandwiched between an anode and a cathode (at least one of them should be transparent) [5, 6, 7, 8, 9]. Recently, the state-of-the-art power conversion efficiencies (PCEs) of single module PSCs in fullerene derivatives system have been boosted up to 11%, which is benefited from the novel materials innovation, the device structure, and fabrication process [10, 11, 12, 13, 14, 15, 16]. However, it still largely lags behind in contrast to inorganic solar cells. Therefore, of particular interest and significance for further driving the PSCs forward is developing the new CP materials and investigation on the correlation between the polymer structure and photovoltaic (PV) performance.

Among various donor materials, more and more attention have paid to the wide band gap (WBG) CPs because of the complementary absorption with some electron acceptors, which can not only broaden the absorption bandwidth of the active layer but also generate a high open circuit voltage (V_{OC}) by reducing the energy loss; thus, a better PCE can be realized by simultaneously obtaining a high short circuit current densities (J_{SC}) and V_{OC} [17, 18, 19]. In the search for constructional units of ideal WBD CPs, we all know that benzo[1,2-*b*:4,5-*b*9]dithiophene (BDT) is a favorable electron-donating constructional unit, which has been used in building

high-efficiency donor polymer materials because of its high stability against oxidation ability, planar molecular skeleton, and ability to easily synthesize [20, 21]. The rigid and large planar conjugated structure of the BDT unit can facilitate to enhance p-p stacking and improve the charge transport performance [20, 22, 23]. Also, thieno[3,2-*b*]thiophene has been demonstrated to be an excellent building block and played a significantly important role in tuning the energy levels and polymer backbone stacking and thus the PV performance [24, 25, 26, 27].

A large quantity of successful optimization designs for CPs primarily originated from polymer backbone modulating, side engineering, and substituents [4, 10, 13, 25, 26, 27, 28]. Apart from the above-mentioned strategies, the substitution positions of polymer, another important and effective method for promoting the PV performance, has been ignored to some content [29, 30, 31, 32, 33, 34]. For example, in 2012, Huang and co-workers reported a series of novel carbazole-based acceptor CPs with different linkage sites (2,7- and 3,6-positions) and found that 2,7-carbazole-derived polymers showed slightly better PCEs than 3,6-carbazole-derived analogues, as a result of a widened absorption range, a deeper highest occupied molecular orbital (HOMO) level, and an improved hole mobility [29]. Following that, Hou and co-workers reported three 2D-BDT-based polymers, PBDTDTBT-*p*, PBDTDTBT-*o*, and PBDTDTBT-*m*, with different alkyl substitution positions, which resulted in different steric hindrance and had a great impact on the PV properties of the corresponding polymers, i.e., V_{OC} varied ranging from 0.67 to 0.90 V and thus PCEs of 3.48–5.76% [30]. Recently, Gao and co-workers changed the substitution positions of IEICO-4F and developed a new acceptor–donor–acceptor-structured nonfullerene acceptor *i*-IEICO-4F; this minor change helped to form the more twisted polymer backbone configuration and resulted in 164 nm blue-shifted absorption to obtain a complementary absorption when blended with J52, thereby achieving the excellent PCE up to 13.18% [31]. These experimental results demonstrated that the substitution positions of materials have a significant influence on the performance of PSCs. Accordingly, it was of importance to further investigate in depth the relationship between substitution positions in CPs and PV performance, which was bound to enrich the donor polymer design and enhance the PCEs of corresponding PV devices.

Considering the above factors, we designed and synthesized two new WBG polymers based on a benzo[1,2-*b*:4,5-*b*9]dithiophene unit attached with the (4,8-bis(4,5-dioctyl-thiophen-2-yl) benzo[1,2-*b*:4,5-*b*9]dithiophene-2,6-diyl)bis(trimethylstannane) (BDT-TSn) and 3,6-dibromothieno[3,2-*b*]thiophene (TT36) or 2,5-dibromothieno[3,2-*b*]thiophene (TT25), named PBDT-TT36 and PBDT-TT25, respectively. We studied the impact of molecular linker positions on their thermal, aggregation, morphological, optical, and PV properties. After the linker positions changed from 3,6-isomer to 2,5-isomer, the optimal inverted polymer solar cells (i-PSCs) exhibited 1.87 times enhancement in PCEs.

Results and discussion

Synthesis and characterization of the copolymers

The synthetic routes of monomers and the copolymers are outlined in Scheme 1. The structures of the monomers were

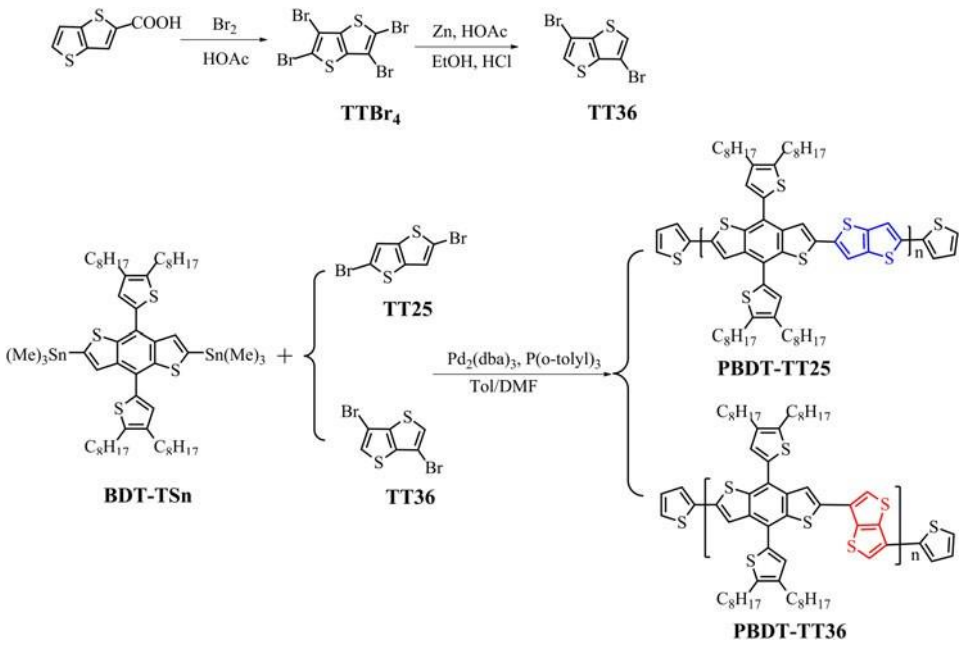

SCHEME 1: Synthesis routes of the monomers and copolymers.

confirmed by ^{1}H NMR before used (Figs. S1 and S2). And the obtained copolymers PBDT-TT25 and PBDT-TT36 were synthesized between TT25 or TT36 and BDT-TSn via the palladium-catalyzed Stille cross-coupling reaction (Scheme 1) [38]. The copolymers were end-capped with 2-tributylstannylthiophene and 2-bromothiophene to remove bromo and trimethylstannyl end groups [39]. After the polymerization, the reaction was cooling to room temperature, and the mixture was precipitated in methanol and filtered. Purification of the precipitated material was carried out by Soxhlet extraction using in sequence acetone, hexane, chloroform, and toluene as the eluants. Then, the concentrated solutions of the copolymers in toluene were poured into methanol again, and the precipitated copolymers were collected with the yields of 75–80%. The copolymers possess good solubility in chloroform, chlorobenzene (CB), and *o*-dichlorobenzene (*o*-DCB). The number average molecular weight (M_n) and PDI were examined by gel permeation chromatography (GPC) using tetrahydrofuran (THF) as the eluant. The results exhibited that the M_n and PDI values were about 19,780 g/mol and 2.05 for PBDT-TT25 and 20,846 g/mol and 2.67 for PBDT-TT36 (Table SI), indicating that the effect generated by different molecular weights could be overlooked.

Thermogravimetric analysis (TGA) measurement was carried out to evaluate the thermal stability of the polymers, and the TGA plots of the two polymers are shown in Fig. S3, and the data are also listed in Table SI. TGA profile reveals that the decompositions temperatures (T_d) at 5% weight loss of the PBDT-TT25 and PBDT-TT36 are about 445 °C and 457 °C under N_2 flow, respectively, indicating that two copolymers have good thermal stability for application in PSCs.

Optical properties and aggregation of the copolymers

A UV-1800 spectrophotometer was used to monitor the ultraviolet–visible light (UV-vis) in solution and solid thin film; the normalized UV-vis absorption spectra and the data of PBDT-TT25 and PBDT-TT36 are shown in Fig. 1 and Table I, respectively. The PBDT-TT25 exhibited two absorption peaks at 352 and 518 nm with a shoulder absorption peak at around 557 nm in dilute CB solution. Compared with that in solution, the absorption spectrum of PBDT-TT25 in solid thin film exhibited relatively similar absorption profile but became greatly broader. It was worth to note that the maximum absorption and onset of the absorption were red-shifted by 8 and 30 nm, respectively, continuing on from solution to solid film, indicating PBDT-TT25 had a better coplanarity and stronger solid stacking interaction. Meanwhile, PBDT-TT36 exhibited similar but significantly blue-shifted absorption profiles in CB solution, i.e., absorption peaks and weak

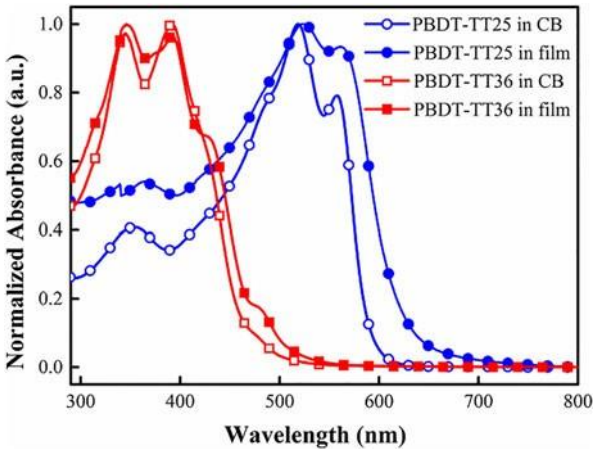

Figure 1: Normalized UV-Vis spectra of the PBDT-TT25 and PBDT-TT36 in diluted CB solution and solid thin film.

shoulder peak were blue-shifted to 344, 391, and 419 nm, respectively, when the linker positions varied from the 2,5-positions to 3,6-positions. And the maximum absorption peak and onset of the absorption were red-shifted by only —1 and 19 nm, respectively, from solution to solid film, implying that there existed relatively weaker molecular interaction [40]. Moreover, the corresponding optical band gap values E_g^{opt} of PBDT-TT25 and PBDT-TT36 were 2.00 and 2.37 eV, respectively, according to the formula E_g^{opt} ¼ 1240=k_{onset}^{film}. These large differences in absorption can explained by more twisted polymer backbone conformation and more nonlinear polymer arrangement obtained in the latter theoretical calculation obvious when the linker positions changed from 2,5- to 3,6-positions.

It is well known that the factors which affect the absorption properties of materials, the extinction coefficient of materials is also an important measure. The molar extinction coefficient (e) of PBDT-TT25 and PBDT-TT36 in *o*-DCB solution was also determined. As shown in Fig. S4, the e at maximum absorption peak (k_{max}) was increased by 23% from 197,686 L/(mol cm) to 243,014 L/(mol cm) after the linker positions varied from 3,6- to 2,5-isomer. These observations suggested that PBDT-TT25 exhibited the greatly widened and enhanced absorption.

To gain insight into the aggregation characteristics of PBDT-TT25 and PBDT-TT36 in solid state, X-ray diffraction (XRD) analyses of the polymers films were carried out, as shown in Fig. 2. In the small angle region, obvious diffraction peaks were observed at 2h 5 4.06° for PBDT-25TT and 2h 5 4.18° for PBDT-TT36, respectively, corresponding to the distance between the polymer interlayer of 21.75 and 21.12 Å. It was noted that PBDT-25TT showed stronger diffraction intensity than PBDT-36TT. Meanwhile, the peaks in the wide angle region reflected the p–p stacking distances between the

TABLE I: Optoelectronic and parameters of the PBDT-TT25 and PBDT-TT36.

Copolymer	k^{soln}_{max} (nm)	k^{soln}_{onset} (nm)	E^{soln}_{g} (eV)	k^{film}_{max} (nm)	k^{film}_{onset} (nm)	E^{opt}_{g} (eV)[a]	u^{onset}_{ox} (eV)	HOMO (eV)[b]	LUMO (eV)[c]
PBDT-TT25	352, 518, 557	589	2.10	362, 526, 560	619	2.00	0.64	—5.33	—3.33
PBDT-TT36	344, 391, 419	504	2.46	347, 390, 429	523	2.37	0.70	—5.39	—3.02

[a]Calculated from the onset of the film absorption $E^{opt}_{g} ¼ 1240=k^{film}_{onset}$.

[b]Calculated from oxidation potential of the copolymer $E_{HOMO} ¼ — u^{onset}_{ox} þ 4:69$ ðeVÞ.

[c]Calculated from the E^{opt}_{g} and HOMO levels of the copolymers $E_{LUMO} ¼ E_{HOMO} þ E^{opt}_{g}$ ðeVÞ.

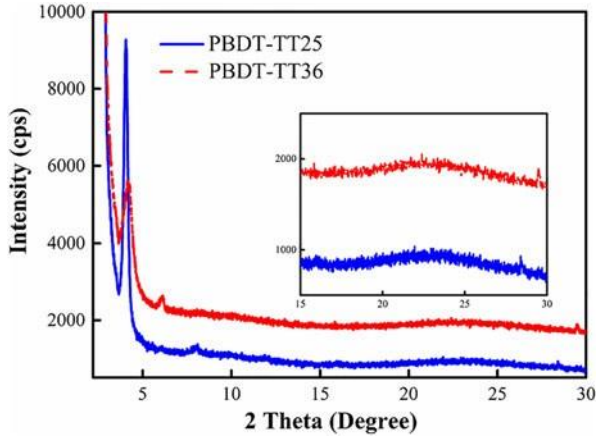

Figure 2: XRD patterns of the pristine PBDT-TT25 and PBDT-36TT.

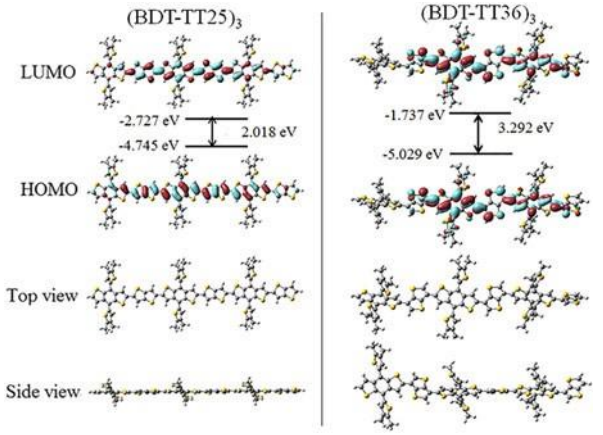

Figure 3: Optimized geometries of each trimer models for BDT-TT25 and BDT-TT36 by DFT at the B3LYP/6-31G* and surface plots and energy levels of frontier orbitals.

polymer backbones, which were located at 2h 5 23.34° for PBDT-25TT and 2h 5 23.07° for PBDT-36TT, respectively, Bragg's law (i.e., k 5 2*d* sin h) [27]. It was not difficult to find that even though PBDT-TT25 possesses a longer interlayer *d*-spacing distance, corresponding to the *d*-spacing of 3.80 and 3.85 Å based on the more important and shorter p-p stacking distance than PBDT-TT36 was observed, suggesting PBDT-TT25 had a more benefited solid molecular stacking interaction and thus obtained higher charge transfer than that of PBDT-TT36.

Theoretical calculation

To further understand the influence of substitution positions on the molecular structures, the electronic properties of the copolymers as well as molecular geometry and orbital distributions of the molecular backbones, quantum chemistry calculations were adopted and used density functional theory (DFT) with the B3LYP/6-31G* level, as implemented in Gaussian 09 [41]. To simplify the calculation process, we selected the model monomers with three repeated donor–acceptor units and substituted the long alkyl side chains with methyl groups. The distributions of HOMO and lowest unoccupied molecular orbital (LUMO) are illustrated in Fig. 3. The HOMO and LUMO frontier orbitals of BDT-TT25 systems were uniformly distributed along the entire conjugated planes. However, the HOMO and LUMO of BDT-TT36 systems were broken at the middle of the thieno[3,2-*b*] thiophene. Moreover, the calculation results showed that HOMO/LUMO/E_g values were —4.745/—2.727/2.018 eV for $(BDT\text{-}TT25)_3$ and —5.029/—1.737/3.292 eV for $(BDT\text{-}TT36)_3$, which were similar with the variation trend observed in the absorption and CV measurements. Additionally, it has been demonstrated that the more linear configuration and more planar backbone structure lead to better charge transfer mobility and thereby increased J_{SC} and PCE of the device. Thus, the optimized ground-state geometries of the $(BDT\text{-}TT25)_3$ and $(BDT\text{-}TT36)_3$ systems are shown in Fig. 3, and the data of dihedral angles are presented in Table SII. We can find that the dihedral angles (U_1 and U_2) between thieno[3,2-*b*] thiophene and BDT-T were 10.89° and 11.19° for $(BDT\text{-}TT25)_3$ and 24.27° and 24.55° for $(BDT\text{-}TT36)_3$. Clearly, the corresponding average twisted angle significantly enlarged (approximately 2.21 times) and the molecular linear configuration also became poor when the linker position changed from 2,5- to 3,6-isomer; these are bad for improving the solar cell property [42, 43, 44]. With a goal of investigating the difference of absorption between the PBDT-TT25 and PBDT-TT36, the calculated UV-vis spectra in $(BDT\text{-}TT25)_3$ and $(BDT\text{-}TT36)_3$ were accomplished, shown in Fig. S5. The calculation results exhibited that the k_{max} was red-shifted by 171 nm from 393 to 564 nm and the e at k_{max} was increased by 60% from 96,451 L/

(mol cm) to 154,664 L/(mol cm) after the linker positions varied from 3,6- to 2,5-isomer, which was consistent with the results from the absorption measurements. These facts can better account for what was the reason for large absorption difference between PBDT-TT25 and PBDT-TT36 aforementioned.

Electrochemical characteristics of the copolymers

It is an important method to measure the electronic energy levels of the CPs with the electrochemical properties determined by cyclic voltammetry (CV) [45, 46]. The onset oxidation potential was determined by the CV curves and calibrated with the potential of ferrocene/ferrocenium (Fc/Fc^{+1}), assumed the energy level of ferrocene/ferrocenium (Fc/Fc^{+1}) to be —4.80 eV below the vacuum level [47]. The redox potential of Fc/Fc^{+1} in the above-mentioned condition was 10.11 V. The cyclic voltammograms of ferrocene and the two polymer films on a glassy carbon electrode in 0.1 mol/L Bu_4NPF_6 acetonitrile solution at a scan rate of 50 mV/s are shown in Fig. 4(a). The onset oxidation potential of PBDT-TT25 and PBDT-TT36 were 0.64 and 0.70 V, respectively [Fig. 4(a)]. The HOMO level and LUMO level, calculated by empirical formulas (E_{HOMO} = —(E_{ox} + 4.69) (eV) [47] and E_{LUMO} = —(|E_{HOMO}| — E_g) (eV), were about —5.33 and —3.33 eV for PBDT-TT25 and —5.39 and —3.02 eV for PBDT-TT36. After the linker positions changed from 2,5-positions to 3,6-positions, the calculated HOMO level showed a decrease from —5.33 to —5.39 eV, as a result of a more twisted planar geometry and weak conjugation from DFT calculation. Furthermore, Fig. 4(b) shows the energy levels diagram of these copolymers and $PC_{61}BM$. It could be found that the E_{LUMO} of all these copolymers were over 0.3 eV larger than that of $PC_{61}BM$, which were capable to provide a sufficient driving force for efficient exciton dissociation at the interface between donor and acceptor [48].

Hole mobility of the copolymers

As known, the carrier charge mobility is an important parameter, which could affect charge separation of the exciton, charge carrier transport, and recombination in the PV devices [49, 50]. The higher mobility will be beneficial to increase the current density and decrease the unfavorable exciton recombination. To investigate the influence of the studied copolymers PBDT-TT25 and PBDT-TT36 with different linker positions on charge carrier transport, the hole mobilities of the copolymers have been measured by space-charge-limited current (SCLC) method with a device structure of ITO/PEDOT:PSS/polymer:$PC_{61}BM$/MoO_3/Ag. The mobilities of the copolymers were calculated by SCLC model, which was described by Eq. (1).

$$\mu = \frac{8L^3 J}{9\varepsilon_0\varepsilon_r V^2} \quad ; \qquad (1)$$

where J stands for current density, L is the film thickness of the active layers, ε_0 is the permittivity of free space, ε_r is the relative dielectric constant of the transport medium, which is assumed to be around 3 for the CPs, V is the internal potential in the devices, and μ is the hole mobility. The thicknesses were 100 nm for PBDT-TT25/$PC_{61}BM$ and 90 nm for PBDT-TT36/$PC_{61}BM$. The J–V characteristics of the devices from the PBDT-TT25/$PC_{61}BM$ and PBDT-TT36/$PC_{61}BM$ blend films are presented in Fig. 5 and the related data are listed in Table II. The hole mobilities were 8.01×10^{-4} $cm^2/(V\,s)$ for PBDT-TT25/$PC_{61}BM$ and 4.30×10^{-4} $cm^2/(V\,s)$ for PBDT-TT36/$PC_{61}BM$. Compared with the counterpart, 1.86 times enhanced SCLC hole mobility in 2,5-linker positions was achieved and benefited from the significant polymer planar configuration, therefore resulting in and explaining an increase in the J_{SC} and fill factor (FF) and thus PCEs from the J–V measurement.

PV properties of the i-PSCs from the copolymers

The PV properties of the two copolymers were explored by using i-PSCs based on the blend film of copolymers with configuration of ITO/PFN/polymer:$PC_{61}BM$/MoO_3/Ag, because the i-PSCs with PFN as cathode modified layers exhibited enhanced stability and performance [51]. The active layers spin-coated from CB solution were composed of PBDT-TT25

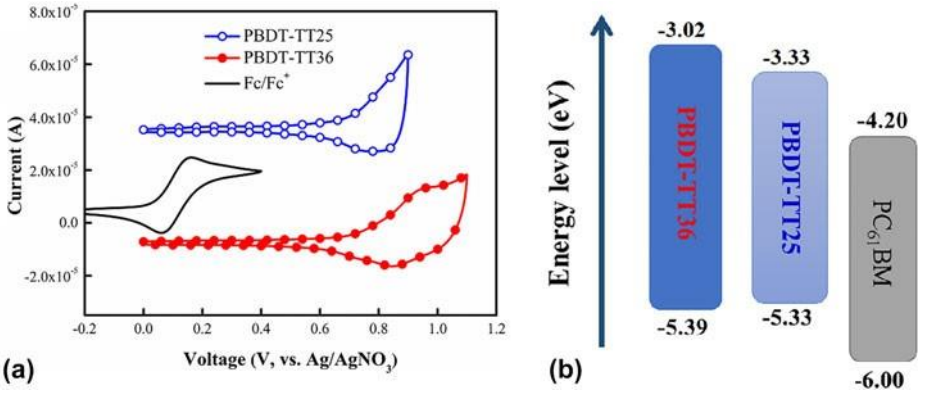

Figure 4: (a) CV curves and (b) energy levels schematic diagram of copolymers.

or PBDT-TT36 as electron donor and fullerene derivatives $PC_{61}BM$ as electron acceptor. The *J*–*V* characteristics and external quantum efficiency (EQE) spectra of inverted devices are shown in Fig. S6, as measured under illumination of AM 1.5G at 100 mW/cm^2 conditions and the corresponding PV performances are listed in Table SIII. The weight ratios of the copolymers to $PC_{61}BM$ in the blend films were varied from 1:1 to 1:1.5 and then to 1:2, and the PCEs of the i-PSCs from PBDT-TT25 were increased from 1.31 to 1.46%, then dropped to 1.30%, while the PCE of the i-PSCs from PBDT-TT36 were increased from 0.16 to 0.44% and then dropped to 0.20%. The optimum *D*/*A* weight ratios of the photosensitive layer were both about 1:1.5, and the device based on PBDT-TT25/$PC_{61}BM$ as the photoactive layer exhibited a higher PCE of 1.46% with a V_{OC} of 0.77 V, a J_{SC} of 4.69 mA/cm^2, and an FF of 40.43%. For PBDT-TT36/$PC_{61}BM$, a PCE of 0.45%, a J_{SC} of 1.55 mA/cm^2, and an FF of 37.84% were observed. Recently, it is widely proved that the solvent additive processing, such as 1,8-diiodoctane (DIO), is an effective way to modify the morphology of photosensitive active layer and improve the PV performance of the CPs [52, 53, 54, 55]. The PCEs of the i-PSCs from PBDT-TT25/$PC_{61}BM$ and PBDT-TT36/$PC_{61}BM$ with optimum weight ratio were correspondingly increased from 1.46 to 1.75% and 0.44 to 0.61% after 3% DIO (V_{DIO}/V_{CB}) was used as solvent additives (Table III, Fig. S6, and Table SIII). It was clear that PBDT-TT25 exhibited a significantly higher PCE than that of PBDT-TT36; this improvement was primarily ascribed to the enhancement of J_{SC} and FF after the linker positions varied from 3,6-positions to 2,5-positions, as a result of the greatly widened and stronger absorption, linear and planar polymer backbone and stronger absorption, and higher SCLC hole mobility.

To confirm the accuracy of the measurement of the PV devices, the corresponding EQE spectra under each condition [Fig. 6(b)] as well as the used device fabrication conditions, including the different blend ratio and additive (Fig. S6), were all measured. As seen from Fig. 6(b), after the linker positions varied from 3,6-positions to 2,5-positions, these experiment results can partially account for greatly increased J_{SC} value of PBDT-TT25. It was also noteworthy that the integrated J_{SC} values from EQE curves were in accordance with those obtained from *J*–*V* evaluations within 3% error.

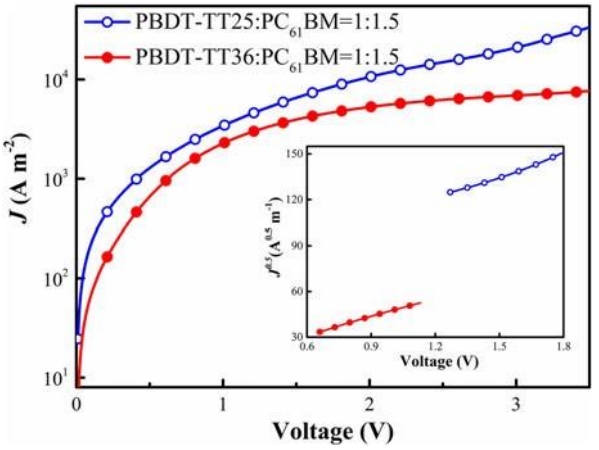

Figure 5: *J*–*V* and $J^{0.5}$–*V* characteristics of the copolymers in the hole-only devices with configuration of ITO/PEDOT:PSS/polymer:$PC_{61}BM$/MoO_3/Ag.

TABLE II: Hole mobilities of blend measured by SCLC model.

Active layer	Ratios (w:w)	Thickness (nm)	Slope	μ_h [cm^2/(V s)]
PBDT-TT25/$PC_{61}BM$	1:1.5	100	48.91	8.01×10^{-4}
PBDT-TT36/$PC_{61}BM$	1:1.5	90	41.97	4.30×10^{-4}

TABLE III: The optimal PV performance of the studied copolymers in i-PSCs.

Blend films	*D*/*A* ratio, additives	V_{OC} (V)	J_{SC} (mA/cm^2)	FF (%)	PCE (%)
PBDT-TT25/$PC_{61}BM$	1:1.5/3%DIO	0.75	4.73 (4.68)[a]	49.25	1.75
PBDT-TT36/$PC_{61}BM$	1:1.5/3%DIO	0.79	1.73 (1.67)[a]	44.37	0.61

[a]The values in the parentheses are the integrated currents obtained from the EQE curves.

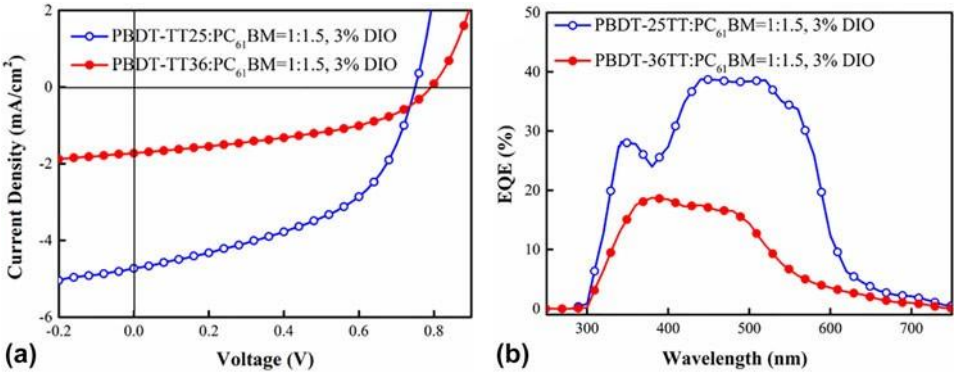

Figure 6: The (a) optimized current density–voltage (*J*–*V*) curves and (b) the EQE spectra of the i-PSCs from the copolymers blend film under AM1.5G illumination (100 mW/cm^2).

Morphological analysis

To understand the reasons for using solvent additives to improve device performance, we used tapping-mode atomic force microscopy (AFM) to investigate the surface morphology of the active layers of copolymers under optimal preparation conditions [26]. As demonstrated by the AFM height images in Fig. S7, for PBDT-TT25/$PC_{61}BM$ the root-mean-square surface roughness (RMS) values greatly decreased from 2.42 to 0.78 nm, which can in part explain the 1.86 times enhanced SCLC hole mobility and thus 22% enhanced FF from 40.43 to 49.25%. For PBDT-TT36/$PC_{61}BM$ blends, the RMS slightly decreases from 0.86 to 0.80 nm. It can be seen the DIO additive has a distinct impact on the PBDT-TT25/$PC_{61}BM$ system but little influence on PBDT-TT36/$PC_{61}BM$ system. Also there was a little difference in the AFM height and phase images between PBDT-TT25/$PC_{61}BM$ and PBDT-TT36/$PC_{61}BM$ (Fig. S8); these AFM measurements observed cannot explain the difference between the studied copolymers with different linker positions.

Conclusions

In conclusion, we have synthesized two benzo[1,2-*b*:4,5-*b*9]dithiophene-based WBG conjugated copolymers PBDT-TT25 and PBDT-TT36 by varying the linker positions of the thieno[3,2-*b*]thiophene unit. Interestingly, it exhibited the greatly widened and stronger absorption and more linear and planar molecular configuration and thus a 1.86 times increase in SCLC hole mobility was achieved even if elevated HOMO energy level when the linker positions changed from 3,6- to 2,5-positions. Thus, these important improvements led a 1.73 times increase in J_{SC} and a 22% enhancement in FF and thus a 1.87 times increase in PCE under similar experimental testing condition. Although the obtained PCEs were unsatisfactory, the disclosed correlation between the property and polymer structure with the varied linker positions was still propitious to design and develop the efficient CP materials in PSCs.

Experiment

Materials

All reagents, unless otherwise specified, were obtained from Aladdin (Shanghai, China), Acros (Belgium, Wisconsin), and TCI Chemical Co. (Shanghai, China), and used as received. $PC_{61}BM$ was purchased from J & K (Beijing, China). All reagents purchased commercially were used without further purification except for THF and toluene, which were dried with sodium with benzophenone as indicator under N_2 flow. The thieno[3,2-*b*]thiophene-2-carboxylicacid [35], 2,5-dibromothieno[3,2-*b*]thiophene (TT25) [35], BDT-TSn [36], and poly[(9,9-bis(39-(*N*,*N*-dimethylamino)propyl)-2,7-fluorene)-*alt*-2,7-(9, 9-dioctylfluorene)] (PFN) [37] were synthesized according to the procedure reported in the references. All the compounds were characterized by ^1H NMR before use.

Synthesis of the monomers and copolymers

Tetrabromothieno[3,2-*b*]thiophene ($TTBr_4$)

To a solution of thieno[3,2-*b*]thiophene-2-carboxylic acid (5.50 g, 30.00 mmol) in acetic acid (300 mL), a solution of Br_2 (48.00 g, 30.00 mmol) was added dropwise at room temperature (r.t.) and stirred for 1 h, then 100 mL of water was added. The solution was heated to reflux and a solution of Br_2 (48.00 g, 30.00 mmol) was added slowly at 120 °C and then stirred for 12 h. After cooling to r.t., 100 mL of water was added. The reaction mixture was extracted with chloroform. The organic phase was washed three times with water (3 × 50 mL), then dried over with Na_2SO_4 and concentrated to afford the brown crude product, which was recrystallized from chloroform and finally obtained a brown solid (10.40 g, 84%).

3,6-Dibromothieno[3,2-*b*]thiophene (TT36)

To a 250 mL three-necked flask, $TTBr_4$ (7.00 g, 15.30 mmol), zinc powder (3.93 g, 61.40 mmol), absolute ethanol (70 mL), water (7 mL), acetic acid (17 mL), and concentrated hydrochloric acid (1.5 mL) were added, and the mixture was heated to 90 °C and stirred for 2 h. After cooling to r.t., the mixture was filtered and the residue was washed with anhydrous ethanol. The reaction mixture was extracted with ethyl acetate. The organic phase was washed three times with dilute aqueous $NaHCO_3$, then dried over anhydrous Na_2SO_4. Ethyl acetate was evaporated under reduced pressure, and the crude product was purified by column chromatography on silica gel using petroleum ether/chloroform (15:1) as eluant, yielding a white solid (2.50 g, 55.6%). Melting point (M.p.): 128–129 °C. ^1H NMR (400 MHz, $CDCl_3$): d (ppm) 7.33 (s, 2H).

2,5-Dibromothieno[3,2-*b*]thiophene (TT25)

The 2,5-dibromo-thieno[3,2-*b*]thiophene (TT25) was synthesized by a procedure adapted from the literature [35]. M.p.: 132–133 °C. ^1H NMR (400 MHz, $CDCl_3$): d (ppm) 7.17 (s, 2H).

PBDT-TT25

TT25 (60 mg, 0.20 mmol), BDT-TSn (230 mg, 0.20 mmol), 10 mL of toluene, and 2 mL of *N*,*N*-dimethylformamide (DMF) were added to a 25 mL two-necked bottle. After being flushed with argon for 20 min, $Pd_2(dba)_3$ (1.5 mg) and P(*o*-tol)$_3$ (2.5 mg) were added as the catalyst, and the mixture was then purged with argon for 10 min. The solution was heated to reflux and stirred for 48 h under argon atmosphere. At the end

of polymerization, the polymer was end-capped with 2-tributylstannylthiophene and 2-bromothiophene to remove bromo and trimethylstannyl end groups. The reaction was cooling to room temperature, and the mixture was precipitated in methanol and filtered. Purification of the precipitated material was carried out by Soxhlet extraction using the sequence acetone, hexane, chloroform, and toluene as the eluants. Toluene was removed under reduced pressure and then poured into methanol (300 mL). The precipitation was collected and dried under vacuum overnight. Yield: 80%. M_n 5 19,778 g/mol with PDI of 2.05. ^{1}H NMR (400 MHz, $CDCl_3$): d (ppm) 8.04 (br, ArH), 7.73–7.33 (br, ArH), 2.98 (m, CH_2), 2.61 (m, CH_2), 1.05–1.81 (m, CH, CH_2), 0.86 (t, CH_3).

PBDT-TT36

The PBDT-TT36 was synthesized as the procedure of PBDT-TT25, except that the polymerization was carried out with BDT-TSn (230 mg, 0.20 mmol) and TT36 (60 mg, 0.20 mmol). Yield: 75%. M_n 5 20,846 g/mol with PDI of 2.67. ^{1}H NMR (400 MHz, $CDCl_3$): d(ppm) 7.52 (br, ArH), 7.37–7.31 (br, ArH), 7.23–7.21 (br, ArH), 2.87 (m, CH_2), 2.69 (m, CH_2), 1.10–1.80 (m, CH, CH_2), 0.85 (t, CH_3).

Acknowledgments

The authors are deeply grateful to the National Nature Science Foundation of China (51463011, 61404067), the Natural Science Foundation of Gansu Province (No. 17JR5RA093), the Foundation of a Hundred Youth Talents Training (152022), and Excellent Team of Scientific Research in Lanzhou Jiaotong University (201705, 201703). We also express our thanks to Instrument Analysis Center of Lanzhou Jiaotong University for related testing support.

Supplementary material

To view supplementary material for this article, please visit https://doi.org/10.1557/jmr.2019.81.

References

1. J.Y. Kim, K. Lee, N.E. Coates, D. Moses, T.Q. Nguyen, M. Dante, and A.J. Heeger: Efficient tandem polymer solar cells fabricated by all-solution processing. *Science* 317, 222 (2007).
2. J.A. Bartelt, Z.M. Beiley, E.T. Hoke, W.R. Mateker, J.D. Douglas, B.A. Collins, J.R. Tumbleston, K.R. Graham, A. Amassian, H. Ade, J.M.J. Fréchet, M.F. Toney, and M.D. McGehee: The importance of fullerene percolation in the mixed regions of polymer-fullerene bulk heterojunction solar cells. *Adv. Energy Mater.* 3, 364 (2013).
3. L. Huo, J. Hou, S. Zhang, H-Y. Chen, and Y. Yang: A polybenzo [1,2-*b*:4,5-*b*9] dithiophene derivative with deep homo level and its application in high-performance polymer solar cells. *Angew. Chem., Int. Ed.* 122, 1542 (2010).
4. H. Zhou, L. Yang, S.C. Price, K.J. Knight, and W. You: Enhanced photovoltaic performance of low-bandgap polymers with deep lumo levels. *Angew. Chem., Int. Ed.* 122, 8164 (2010).
5. J. Li, Z. Liang, Y. Wang, H. Li, J. Tong, X. Bao, and Y. Xia: Enhanced efficiency of polymer solar cells through synergistic optimization of mobility and tuning donor alloys by adding high-mobility conjugated polymers. *J. Mater. Chem. C* 6, 11015 (2018).
6. W. Chen, G. Huang, X. Li, H. Wang, Y. Li, H. Jiang, N. Zheng, and R. Yang: Side-chain-promoted benzodithiophene-based conjugated polymers toward striking enhancement of photovoltaic properties for polymer solar cells. *ACS Appl. Mater. Interfaces* 10, 42747 (2018).
7. W. Chen, H. Jiang, G. Huang, J. Zhang, M. Cai, X. Wan, and R. Yang: High-Efficiency ternary polymer solar cells based on intense FRET energy transfer process. *Sol. RRL* 2, 1800101 (2018).
8. J. Li, Y. Wang, Z. Liang, N. Wang, J. Tong, C. Yang, X. Bao, and Y. Xia: Enhanced organic photovoltaic performance through modulating vertical composition distribution and promoting crystallinity of the photoactive layer by diphenyl sulfide additive. *ACS Appl. Mater. Interfaces* 11, 7022 (2019).
9. G. Yu, J. Gao, J.C. Hummelen, F. Wudi, and A.J. Heeger: Polymer photovoltaic cells: Enhanced efficiencies via a network of internal donor-acceptor heterojunctions. *Science* 270, 1789 (1995).
10. Y. Liu, J. Zhao, Z. Li, C. Mu, W. Ma, H. Hu, K. Jiang, H. Lin, H. Ade, and H. Yan: Aggregation and morphology control enables multiple cases of high-efficiency polymer solar cells. *Nat. Commun.* 5, 5293 (2014).
11. S. Zhang, L. Ye, W. Zhao, B. Yang, Q. Wang, and J. Hou: Realizing over 10% efficiency in polymer solar cell by device optimization. *Sci. China: Chem.* 58, 248 (2015).
12. Z. He, B. Xiao, F. Liu, H. Wu, Y. Yang, S. Xiao, C. Wang, T.P. Russell, and Y. Cao: Single-junction polymer solar cells with high efficiency and photovoltage. *Nat. Photonics* 9, 173 (2015).
13. J.R. Tumbleston, B.A. Collins, L. Yang, A.C. Stuart, E. Gann, W. Ma, W. You, and H. Ade: The influence of molecular orientation on organic bulk heterojunction solar cells. *Nat. Photonics* 8, 385 (2014).
14. G. Zhang, K. Zhang, Q. Yin, X. Jiang, Z. Wang, J. Xin, W. Ma, H. Yan, F. Huang, and Y. Cao: High-performance ternary organic solar cell enabled by a thick active layer containing a liquid crystalline small molecule donor. *J. Am. Chem. Soc.* 139, 2387 (2017).
15. M. Li, K. Gao, X. Wan, Q. Zhang, B. Kan, R. Xia, F. Liu, X. Yang, H. Feng, W. Ni, Y. Wang, J. Peng, H. Zhang, Z. Liang, H. Yip, X. Peng, Y. Cao, and Y. Chen: Solution-processed organic tandem solar cells with power conversion efficiencies ~ 12%. *Nat. Photonics* 11, 85 (2016).

16. J. Zhao, Y. Li, G. Yang, K. Jiang, H. Lin, H. Ade, W. Ma, and H. Yan: Efficient organic solar cells processed from hydrocarbon solvents. *Nat. Energy* 1, 15027 (2016).
17. Y. An, X. Liao, L. Chen, J. Yin, Q. Ai, Q. Xie, B. Huang, A.K.Y. Jen, and Y. Chen: Nonhalogen solvent-processed asymmetric wide-bandgap polymers for nonfullerene organic solar cells with over 10% efficiency. *Adv. Funct. Mater.* 28, 1706517 (2018).
18. L. Lan, Z. Chen, Q. Hu, L. Ying, R. Zhu, F. Liu, T.P. Russell, F. Huang, and Y. Cao: High-performance polymer solar cells based on a wide-bandgap polymer containing pyrrolo[3,4-*f*] benzotriazole-5,7-dione with a power conversion efficiency of 8.63%. *Adv. Sci.* 3, 1600032 (2016).
19. K. Feng, G. Yang, X. Xu, G. Zhang, H. Yan, O. Awartani, L. Ye, H. Ade, Y. Li, and Q. Peng: Realizing over 13% efficiency in green-solvent-processed nonfullerene organic solar cells enabled by 1,3,4-thiadiazole-based wide-bandgap copolymers. *Adv. Energy Mater.* 8, 1602773 (2018).
20. Y. Cai, L. Huo, and Y. Sun: Recent advances in wide-bandgap photovoltaic polymers. *Adv. Mater.* 29, 1605437 (2017).
21. H. Pan, Y. Wu, Y. Li, P. Liu, B.S. Ong, S. Zhu, and G. Xu: Benzodithiophene copolymer-a low-temperature, solution-processed high-performance semiconductor for thin-film transistors. *Adv. Funct. Mater.* 17, 3574 (2007).
22. C. Wang, H. Dong, W. Hu, Y. Liu, and D. Zhu: Semiconducting p-conjugated systems in field-effect transistors: A material odyssey of organic electronics. *Chem. Rev.* 112, 2208 (2012).
23. H. Yao, L. Ye, H. Zhang, S. Li, S. Zhang, and J. Hou: Molecular design of benzodithiophene-based organic photovoltaic materials. *Chem. Rev.* 116, 7397 (2016).
24. I. McCulloch, M. Heeney, C. Bailey, K. Genevicius, I. Macdonald, M. Shkunov, D. Sparrowe, S. Tierney, R. Wagner, W. Zhang, M.L. Chabinyc, R.J. Kline, M.D. Mcgehee, and M.F. Toney: Liquid-crystalline semiconducting polymers with high charge-carrier mobility. *Nat. Mater.* 5, 328 (2006).
25. S. Zhang, B. Yang, D. Liu, H. Zhang, W. Zhao, Q. Wang, C. He, and J. Hou: Correlations among chemical structure, backbone conformation, and morphology in two highly efficient photovoltaic polymer materials. *Macromolecules* 49, 120 (2016).
26. Y. Jin, Z. Chen, S. Dong, N. Zheng, L. Ying, X. Jiang, F. Liu, F. Huang, and Y. Cao: A novel naphtho[1,2-*c*:5,6-*c*9]bis([1,2,5] thiadiazole)-based narrow bandgap p-conjugated polymer with power conversion efficiency over 10%. *Adv. Mater.* 28, 9811 (2016).
27. J. Tong, J. Li, P. Zhang, X. Ma, M. Wang, L. An, J. Sun, P. Guo, C. Yang, and Y. Xia: Naphtho[1,2-*c*:5,6-*c*9]bis[1,2,5]-thiadiazole-based conjugated polymers consisting of oligothiophenes for efficient polymer solar cells. *Polymer* 121, 183 (2017).
28. H. Zhou, L. Yang, and W. You: Rational design of high performance conjugated polymers for organic solar cells. *Macromolecules* 45, 607 (2012).
29. H. Xie, K. Zhang, C. Duan, S. Liu, F. Huang, and Y. Cao: New acceptor-pended conjugated polymers based on 3,6- and 2,7-carbazole for polymer solar cells. *Polymer* 53, 5675 (2012).
30. H. Yao, L. Ye, L. Huo, and J. Hou: Influence of the alkyl substitution position on photovoltaic properties of 2D-BDT-based conjugated polymers. *Sci. China Mater.* 58, 213 (2015).
31. W. Wang, B. Zhao, Z. Cong, Y. Xie, C. Gao, H. Wu, and Y. Cao: Nonfullerene polymer solar cells based on a main-chain twisted low-bandgap acceptor with power conversion efficiency of 13.2%. *ACS Energy Lett.* 3, 1499 (2018).
32. T.H. Le, Q.D. Dao, M.P. Nghiêm, S. Péralta, R. Guillot, Q.N. Pham, A. Fujii, M. Ozaki, F. Goubard, and T-T. Bui: Triphenylamine–thienothiophene organic charge-transport molecular materials: Effect of substitution pattern on their thermal, photoelectrochemical, and photovoltaic properties. *Chem.–Asian J.* 13, 1302 (2018).
33. X. Liu, F. Kong, R. Ghadari, S. Jin, W. Chen, T. Yu, T. Hayat, A. Alsaedi, F. Guo, Z. Tan, J. Chen, and S. Dai: Thiophene-arylamine hole-transporting materials in perovskite solar cells: Substitution position effect. *Energy Technol.* 5, 1788 (2017).
34. R. Singh, G. Pagona, V.G. Gregoriou, N. Tagmatarchis, D. Toliopoulos, Y. Han, Z. Fei, A. Katsouras, A. Avgeropoulos, T.D. Anthopoulos, M. Heeney, P.E. Keivanidis, and C. L. Chochos: The impact of thienothiophene isomeric structures on the optoelectronic properties and photovoltaic performance in quinoxaline based donor-acceptor copolymers. *Polym. Chem.* 6, 3098 (2015).
35. E. Lim, B.J. Jung, and H.K. Shim: Synthesis and characterization of a new light-emitting fluorene-thieno[3,2-*b*]thiophene-based conjugated copolymer. *Macromolecules* 36, 4288 (2003).
36. P. Gao, J. Tong, P. Guo, J. Li, N. Wang, C. Li, X. Ma, P. Zhang, C. Wang, and Y. Xia: Medium band gap conjugated polymers from thienoacene derivatives and pentacyclic aromatic lactam as promising alternatives of poly(3-hexylthiophene) in photovoltaic application. *J. Polym. Sci., Part A: Polym. Chem.* 56, 85 (2018).
37. D. Zhu, X. Bao, Q. Zhu, C. Gu, M. Qiu, S. Wen, J. Wang, B. Shahida, and R. Yang: Thienothiophene-based copolymers for high-performance solar cells, employing different orientations of the thiazole group as a p bridge. *Energy Environ. Sci.* 10, 614 (2017).
38. M. An, F. Xie, X. Geng, J. Zhang, J. Jiang, Z. Lei, D. He, Z. Xiao, and L. Ding: A high-performance D–A copolymer based on dithieno[3,2-*b*:29,39-*d*] pyridin-5(4h) -one unit compatible with fullerene and nonfullerene acceptors in solar cells. *Adv. Energy Mater.* 7, 1602509 (2017).
39. N. Blouin, A. Michaud, and M. Leclerc: A low-bandgap poly(2,7-carbazole) derivative for use in high-performance solar cells. *Adv. Mater.* 19, 2295 (2007).
40. H. Zhang, S. Ying, B. Tieke, J. Zhang, and W. Yang: 1,6-Naphthodipyrrolidone -based donor–acceptor polymers with low bandgap. *Polymer* 60, 215 (2015).

41. M.J. Frisch, G.W. Trucks, H.B. Schlegel, G.E. Scuseria, M. A. Robb, J.R. Cheeseman, G. Scalmani, V. Barone, B. Mennucci, G.A. Petersson, H. Nakatsuji, M. Caricato, X. Li, H.P. Hratchian, A.F. Izmaylov, J. Bloino, G. Zheng, J.L. Sonnenberg, M. Hada, M. Ehara, K. Toyota, R. Fukuda, J. Hasegawa, M. Ishida, T. Nakajima, Y. Honda, O. Kitao, H. Nakai, T. Vreven, J. A. Montgomery, Jr., J.E. Peralta, F. Ogliaro, M. Bearpark, J. J. Heyd, E. Brothers, K.N. Kudin, V.N. Staroverov, R. Kobayashi, J. Normand, K. Raghavachari, A. Rendell, J.C. Burant, S. S. Iyengar, J. Tomasi, M. Cossi, N. Rega, J.M. Millam, M. Klene, J. E. Knox, J.B. Cross, V. Bakken, C. Adamo, J. Jaramillo, R. Gomperts, R.E. Stratmann, O. Yazyev, A.J. Austin, R. Cammi, C. Pomelli, J.W. Ochterski, R.L. Martin, K. Morokuma, V. G. Zakrzewski, G.A. Voth, P. Salvador, J.J. Dannenberg, S. Dapprich, A.D. Daniels, Ö. Farkas, J.B. Foresman, J.V. Ortiz, J. Cioslowski, and D.J. Fox: *Gaussian 09, Revision A.01* (Gaussian, Inc., Wallingford, Connecticut, 2009).
42. Y. Wu, Z. Li, W. Ma, Y. Huang, and J. Hou: PDT-S-T: A new polymer with optimized molecular conformation for controlled aggregation and p-p stacking and its application in efficient photovoltaic devices. *Adv. Mater.* 25, 3449 (2013).
43. J. Yu, Q. An, J. Hai, X. Nie, and W. Tang: Thiadiazole quinoxaline-based copolymers with ; 1.0 eV bandgap for ternary polymer solar cells. *Polymer* 79, 12 (2015).
44. D. Liu, J. Wang, C. Gu, Y. Li, X. Bao, and R. Yang: Stirring up acceptor phase and controlling morphology via choosing appropriate rigid aryl rings as lever arms in symmetry-breaking benzodithiophene for high-performance fullerene and fullerene-free polymer solar cells. *Adv. Mater.* 30, 1705870 (2018).
45. Y. Li, Y. Cao, J. Gao, D. Wang, G. Yu, and A.J. Heeger: Electrochemical properties of luminescent polymers and polymer light-emitting electrochemical cells. *Synth. Met.* 99, 243 (1999).
46. Q. Sun, H. Wang, C. Yang, and Y. Li: Synthesis and electroluminescence of novel copolymers containing crown ether spacers. *J. Mater. Chem.* 13, 800 (2003).
47. J. Pommerehne, H. Vestweber, W. Guss, R.F. Mahrt, H. Bässler, M. Porsch, and J. Daub: Efficient two layer leads on a polymer blend basis. *Adv. Mater.* 7, 551 (1995).
48. Y. Li: Molecular design of photovoltaic materials for polymer solar cells: Toward suitable electronic energy levels and broad absorption. *Acc. Chem. Res.* 45, 723 (2012).
49. G.G. Malliaras, P.J. Brock, C. Scott, and J.R. Salem: Electrical characteristics and efficiency of single-layer organic light-emitting diodes. *Phys. Rev. B* 58, R13411 (1998).
50. Y. Hu, Z. Li, L. Jiang, Z. Chen, L. Liao, and E. Wang: Correlation of molecular structure and charge transport properties: A case study in naphthalenediimide-based copolymer semiconductors. *Adv. Electron. Mater.* 4, 1800203 (2018).
51. A.K. Kyaw, D.H. Wang, C. Luo, Y. Cao, T.Q. Nguyen, G. C. Bazan, and A.J. Heeger: Effects of solvent additives on morphology, charge generation, transport, and recombination in solution-processed small-molecule solar cells. *Adv. Energy Mater.* 4, 1301469 (2014).
52. T-Y. Chu, Y-H. Lee, and O.K. Song: Effects of interfacial stability between electron transporting layer and cathode on the degradation process of organic light-emitting diodes. *Appl. Phys. Lett.* 91, 223509 (2007).
53. Y. Xia, H. Zhang, J. Li, J. Tong, P. Zhang, and C. Yang: Synthesis of dithieno[2,3-*d*:2′,3′-*d*′]benzo[1,2-*b*:4,5-*b*′]dithiophene-alt-isoindigo conjugated polymer and enhancement of photovoltaic property with diphenyl sulfide additives. *J. Polym. Res.* 22, 633 (2015).
54. H. Li, D. He, P. Mao, Y. Wei, L. Ding, and J. Wang: Additive-free organic solar cells with power conversion efficiency over 10%. *Adv. Energy Mater.* 7, 1602663 (2017).
55. J. Tong, L. An, J. Li, J. Lv, P. Guo, L. Li, P. Zhang, C. Yang, Y. Xia, and C. Wang: Effects of alkyl side chain length of low bandgap naphtho[1,2-*c*:5,6-*c*′]bis[1,2,5]thiadiazole based copolymers on the optoelectronic properties of polymer solar cells. *J. Polym. Sci., Part A: Polym. Chem.* 56, 2059 (2018).